Materials Today Chemistry 22 (2021) 100618

Contents lists available at ScienceDirect

Materials Today Chemistry

journal homepage: www.journals.elsevier.com/materials-today-chemistry/

Anticancer therapeutic efficacy of biogenic *Am*-ZnO nanoparticles on 2D and 3D tumor models

S.C. Chabattula [a, n], P.K. Gupta [b, **, n], S.K. Tripathi [c], R. Gahtori [d], P. Padhi [e], S. Mahapatra [f], B.K. Biswal [c], S.K. Singh [g], K. Dua [h, m], J. Ruokolainen [k], Y.K. Mishra [i], N.K. Jha [j], D.K. Bishi [e, ***], K.K. Kesari [k, l, *]

[a] *Stem Cell and Molecular Biology Lab, Department of Biotechnology, Indian Institute of Technology Madras, Chennai, 600036, Tamil Nadu, India*
[b] *Department of Life Sciences, School of Basic Sciences and Research, Sharda University, Plot No. 32 − 34, Knowledge Park III, Greater Noida, 201310, Uttar Pradesh, India*
[c] *Cancer Drug Resistance Laboratory, Department of Life Science, National Institute of Technology Rourkela, Rourkela, 769008, Odisha, India*
[d] *Department of Biotechnology, Sir J.C. Bose Technical Campus, Kumaun University, Nainital, 263136, Uttarakhand, India*
[e] *Department of Biotechnology, Rama Devi Women's University, Bhubaneswar, 751022, Odisha, India*
[f] *Department of Botany, Rama Devi Women's University, Bhubaneswar, 751022, Odisha, India*
[g] *School of Pharmaceutical Sciences, Lovely Professional University, Phagwara, Punjab, 144411, India*
[h] *Discipline of Pharmacy, Graduate School of Health, University of Technology Sydney, NSW, 2007, Australia*
[i] *Smart Materials, NanoSYD, Mads Clausen Institute, University of Southern Denmark, Alsion 2, DK-6400, Sønderborg, Denmark*
[j] *Department of Biotechnology, School of Engineering & Technology (SET), Sharda University, Greater Noida, 201310, UP, India*
[k] *Department of Applied Physics, School of Science, Aalto University, Espoo, 00076, Finland*
[l] *Department of Bioproducts and Biosystems, School of Chemical Engineering, Aalto University, Espoo, 00076, Finland*
[m] *Faculty of Health, Australian Research Centre in Complementary and Integrative Medicine, University of Technology Sydney, Ultimo, New South Wales, 2007 Australia*

A R T I C L E I N F O

Article history:
Received 24 June 2021
Received in revised form
4 September 2021
Accepted 27 September 2021
Available online xxx

Keywords:
ZnO
Nanoparticles
Anti-cancer
Apoptosis
Leaf's extract
Annona muricata

A B S T R A C T

The present study fabricates biogenic zinc oxide nanoparticles (ZnO NPs) with the aqueous leaf extract of *Annona muricata* (*Am*) plant collected from semi-evergreen forests of Odisha, India. The synthesized *Am*-ZnO NPs were physicochemically characterized. The ultraviolet/visible spectrum showed the maximum optical absorbance of *Am*-ZnO NPs at 355 nm. High-resolution transmission electron microscopy analysis presented the nearly spherical shape of *Am*-ZnO NPs with an average particle size of 80 nm. The net surface charge and hydrodynamic size of *Am*-ZnO NPs were measured to be ~−2.59 mV and ~417 nm, respectively. *Am*-ZnO NPs were found to be biocompatible and hemocompatible nature. Furthermore, *Am*-ZnO NPs displayed strong anticancer effects on both 2D and 3D tumor models. We observed a dose-dependent toxicity on both A549 and MOLT4 cells and observed a size reduction in the A549 tumor spheroids. Subsequently, we observed a depolarization in mitochondrial membrane potential of *Am*-ZnO NP−treated cancer cells leading to the apoptosis induction in cancer cells.

1. Introduction

In 21st century, the nanoparticle (NP) research is emerging globally with unique properties. These particles have multiple applications in the different fields of scientific community. Nanoparticles are either organic or inorganic nature, and they have been synthesized by different physical, chemical, and biological methods [1]. The organic NPs are polymeric NPs, lipid NPs, protein NPs, and carbohydrate NPs while the inorganic NPs are metal-oxide NPs, carbon structures−based NPs, and mesoporous silica NPs [1]. Among inorganic NPs, metals and metal

* Corresponding author.
** Corresponding author.
*** Corresponding author.
E-mail addresses: dr.piyushkgupta@gmail.com, piyush.kumar1@sharda.ac.in (P.K. Gupta), dillipkumar.bishi@gmail.com (D.K. Bishi), kavindra.kesari@aalto.fi (K.K. Kesari).
[n] Both authors contributed equally as first author.

https://doi.org/10.1016/j.mtchem.2021.100618

oxides—based NPs contribute a significant role in various fields such as drug delivery, bioimaging, biosensing, bioelectronic, and tissue engineering applications [2]. The metal-oxide NPs also display the strong antibacterial, antifungal, antimalarial, anticancer, and photocatalytic activities [3,4]. Usually, the synthesis of metal-oxide NPs via the green approach is more favorable than their chemical synthesis because the chemical approach requires the excess use of organic solvents and toxic chemicals. In addition, high temperature and pressure are required during the chemical synthesis. Therefore, the green synthesis is a valuable alternative of chemical synthesis and leads to the production of non-toxic metal-oxide NPs [5–7]. In recent years, the use of phytocompounds received more attention for the green synthesis of metal-oxide NPs. These natural compounds are traditionally well-known for their medicinal uses without any side-effects. In fact, phytocompounds play a major role in cancer prevention and treatment [8].

Amongst metal-oxide NPs, ZnO NPs could be easily fabricated using phytoextracts. These stabilized and capped NPs are non-toxic and ecofriendly in nature. These NPs exhibit strong antifungal, antibacterial, antidiabetic, antioxidant, anticancer and photocatalytic activities [9,27]. In 2015, the Food and Drug Administration approved ZnO NPs as a safer material. *Annona muricata* (*Am*) is a small evergreen tree, commonly known as Graviola belongs to Annonaceae family. It is an important herbal medicine of medicinal science. This plant has a long history of traditional uses such as antimicrobial, anticancer, and anti-inflammatory activities [10]. In 2014, Pieme et al. reported the antiproliferative and pro-apoptotic activity of *Am*-extract against human cancer cells [11]. In 2018, Chamcheu et al. displayed the antiproliferative and anti-colonogenic effect of *Am*-extract against human non-melanoma skin cancer [12].

In recent years, various studies reported the biogenic synthesis of ZnO NPs using plant extracts and displayed their excellent activity in biomedical and environmental applications [40–42,45]. In 2021, Ramesh et al. [40] fabricated biocompatible ZnO NPs using *Cassia auriculatacan* leaf extract and showed their high bactericidal activity against *Bacillus subtilis, Klebsiella pneumonia, Pseudomonas aeruginosa,* and *Proteus mirabilis*. In 2021, Vinayagam et al. [41] prepared ZnO nanoflowers (ZnONFs) using the pd extract of *Peltophorum pterocarpum* and showed the photocatalytic role of these nanoflowers to remove the inorganic pollutants like methylene blue in solar light. Also, in 2021, Pachaiappan et al. [42] synthesized ZnO NPs using the leaf extract of *Justicia adhatoda* plant, and they found the growth inhibition of different bacterial and fungal strains by the release of Zn ions and production of reactive oxygen species (ROS) which could kill these microbes. In previous studies, *Am*-extract has been used to fabricate silver NPs and lipid NPs [13,14] but no reports are available on *Am*-extract—assisted ZnO NP's synthesis. Moreover, the anticancer therapeutic effect of *Am*-ZnO NPs has not investigated so far. Thereby, in this study, the synthesis of *Am*-ZnO NPs has been reported for the first-time to the best of our literature knowledge. These biocompatible and hemocompatible Am-ZnO NPs have been physicochemically characterized via Fourier transform infra-red (FTIR), ultraviolet (UV)—visible, X-ray diffractometer (XRD), high-resolution transmission electron microscopy (HR-TEM) and dynamic light scattering (DLS) analysis in detail. Furthermore, we have investigated the anticancer effects of *Am*-ZnO NPs on 2D (A549, MOLT4) and 3D (A549) tumor models. In addition, the mechanism of cancer cell death induced by *Am*-ZnO NPs is investigated and understood in detail which is going to open many new avenues in caner nanotechnology.

2. Materials and methods

2.1. Materials

2.1.1. Chemical reagents and glasswares

Chemical reagents like sodium hydroxide, zinc acetate dihydrate, doxorubicin hydrochloride (DOX-HCl), and organic solvents were procured Merck, India. Glassware was acquired from Borosil, India.

2.1.2. Cell culture reagents and plasticwares

3T3 cells (mouse fibroblast cells), MOLT4 cells (human T lymphoid cells), and A549 cells (human lung cancer cells) were purchased from National Centre for Cell Science, India. These cells were maintained in 10% fetal bovine serum (FBS) containing Dulbecco's Modified Eagle Medium (DMEM) and Roswell Park Memorial Institute (RPMI) media (Gibco, USA) in a humidified CO_2 incubator (Thermo Scientific, USA) at 37 °C. The Annexin-V FITC/PI stain and JC-1 stain were purchased from Abcam, UK. The cell culture plastics were procured from Corning, USA.

2.2. Methods

2.2.1. Preparation of Am leaf extract

Fresh leaves of *Am* were collected from the Ganjam area of Ganjam District, Odisha, India. These leaves were cleaned with water and dried for 5 days at room temperature. Then, leaves were grinded in an electric blender and prepared the fine powder. Furthermore, 5 g leaf powder was suspended in 50 mL distilled water. The prepared aqueous extract was boiled for 4 h at 100 °C. After 15 min, the aqueous solution was filtered using the Whatman (No. 1) paper and the collected filtered solution stored at 4 °C for further use [15].

2.2.2. Fabrication of Am-ZnO NPs

Zinc acetate dihydrate is the starting compound for ZnO NP's synthesis as described previously in a report [16]. Briefly, 0.02 M concentration of zinc acetate dihydrate was added into 50 mL of distilled water and kept under constant stirring. Then, 1 mL aqueous leaf extract of *Am* plant was mixed in the zinc acetate dihydrate solution. Later, 2 M NaOH was added in the same solution to reach the solution pH = 12 and continuously allowed for stirring for 2 h. The resulting pale white precipitate was obtained after centrifugation at 15,000 rpm and washed with ethanol for removing the impurities. The obtained white precipitate was kept in an empty vial and dried at 60 °C in hot air oven for overnight. Finally, the powdered form of *Am*-ZnO NPs was stored for further use.

2.2.3. Physicochemical characterizations of Am-ZnO NPs

The optical properties of *Am*-ZnO NPs were analyzed by JASCO V-630 UV/visible spectroscopy (JASCO, USA) in a wavelength range of 200–800 nm. Next, the crystalline nature of dried *Am*-ZnO NPs was determined using powder XRD (Bruker, Germany). The X-ray diffraction pattern was recorded between 20º and 80º. Furthermore, the phytocompounds present on synthesized *Am*-ZnO NPs were analyzed by FTIR spectroscopy (JASCO, USA) using the KBr pellet technique. The FTIR spectra was recorded between 500 and 4,000 cm^{-1}. The HR-TEM was used to calculate the particle size and shape in the dry state. The field-emission scanning electron microscopy (FE-SEM) was used for the surface analysis of *Am*-ZnO NPs. The particle size of *Am*-ZnO NPs were analyzed by Image J software (NIH, USA), and a particle size distribution graph of *Am*-

ZnO NPs was plotted using the Gaussian fitting curve. The selected area electron diffraction (SAED) pattern analysis was used to analyze the structural information of *Am*-ZnO NPs. Then, the Zetasizer Nano ZS instrument was used to calculate the average zeta potential (net charge on NP's surface), average hydrodynamic size ($Z_{Average}$), and polydispersity index (PDI) values of *Am*-ZnO NPs in aqueous solution. Next, the stability of *Am*-ZnO NPs were studied with respect to time for 15 days in 10% serum containing DMEM media simulating the internal environment of the human body. At each 5 days' time-interval, the Zetasizer Nano ZS instrument was used to calculate the average hydrodynamic size and PDI values of the incubated *Am*-ZnO NPs.

2.2.4. Biocompatibility

The biocompatible nature of *Am*-ZnO NPs was analyzed by the MTT test on 3T3 cells. During this experiment, 3T3 cells were incubated with different concentrations (between 7.81 μg/mL and 500 μg/mL) of *Am*-ZnO NPs till 72 h along with a negative control. Thereafter, all the steps of the MTT test were followed in a similar way as reported in our earlier studies [17,18]. The cell viability was calculated, and the cytotoxic effects of *Am*-ZnO NPs were examined on 3T3 cells.

2.2.5. Hemocompatibility

The hemocompatible nature of ZnO and *Am*-ZnO NPs was analyzed on 2% red blood cell (RBC) suspension of human blood collected from the blood bank of Sharda Hospital, Greater Noida, India. During this experiment, RBCs were incubated with different concentrations (between 0.62 mg/mL and 10 mg/mL) of *Am*-ZnO NPs till 4 h along with a positive and negative control. Next, all the steps of the hemocompatibility test were followed in a similar way as reported in our earlier studies [17,18]. The percentages of hemolysis were calculated, and an image of the collected supernatants was captured with a camera (Nikon, Japan).

2.2.6. Anticancer effects on 2D and 3D tumor models

The anticancer effects of ZnO NPs and *Am*-ZnO NPs on 2D tumor models were studied by the MTT test. The experiment was carried out on both 2D culture of A549 and MOLT4 cells. During the experiment, 5000 A549 cells and 10,000 MOLT4 cells were seeded in each well of a 96-well plate and then treated with different concentrations (between 7.81 μg/mL and 500 μg/mL) of ZnO NPs and *Am*-ZnO NPs. In this experiment, DOX-HCl was used as a positive control. Both cells were also treated with different concentrations (between 1.56 μg/mL and 100 μg/mL) of DOX-HCl. After treatment, all the steps of MTT test were followed in a similar way as reported in our earlier studies [17,18]. The treated cells were incubated for 12, 24, and 48 h. Then, the cell viability was calculated, and the half-maximal inhibitory concentration (IC_{50}) values of both treatments were calculated at 24 h by plotting their dose-responsive graphs.

The anticancer effect of *Am*-ZnO NPs on 3D tumor models was studied by calculating the average diameter of treated A549 tumor spheroids [18]. These uniform diameter spheroids were treated with IC_{50} values of both *Am*-ZnO NPs and DOX-HCl. After treatment, all the steps of *ex vivo* test were followed in a similar way as reported in our earlier study [18]. The untreated spheroids were kept as negative control during the experiment. The images were captured by phase contrast microscope at 4× magnification till 72 h. In addition, the diameter of these spheroids was measured using Image J software (NIH, USA).

2.2.7. Evaluation of cancer cell death mechanism by apoptosis assay

The cancer cell death mechanism was studied through apoptosis assay using Annexin-V FITC/PI staining kit by flow cytometry instrument. In this experiment, 5000 A549 cells were treated with ½ IC_{50} and IC_{50} values of both *Am*-ZnO NPs and DOX-HCl and incubated for next 24 h. After treatment, all the steps of apoptosis assay were followed in a similar way as reported in our earlier study [17]. The total percentages of live cells, apoptotic cells, and necrotic cells were calculated in both treatments using the scatter plot data. The histogram was plotted between the cell populations and apoptotic phases.

2.2.8. Mitochondrial membrane potential (MMP) assay by JC-1 staining

The change in the MMP is a pre-apoptosis event. Such changes were measured by flow cytometry using JC-1 dye. In this experiment, 5000 A549 cells were treated with ½ IC_{50} and IC_{50} values of both *Am*-ZnO NPs and DOX-HCl and incubated for next 24 h. After

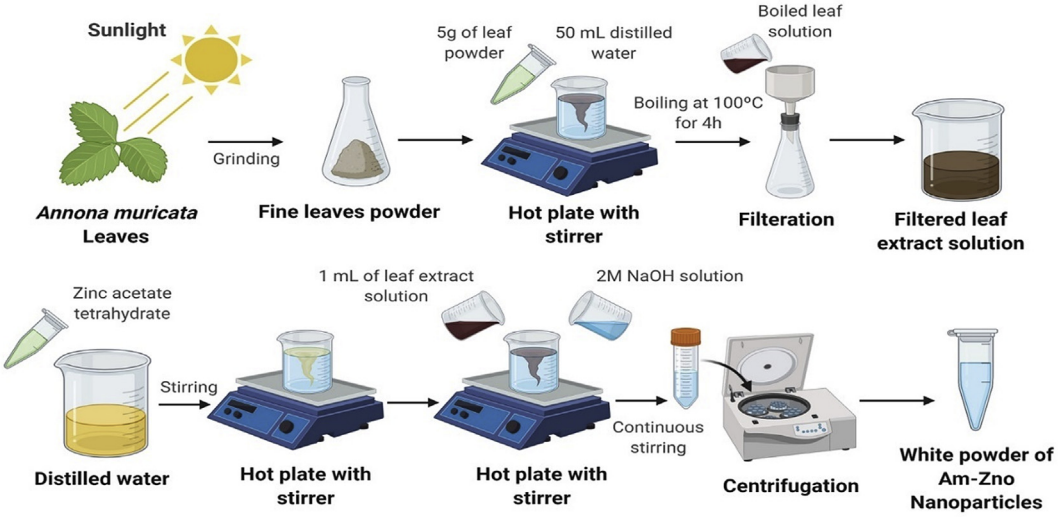

Fig. 1. Schematic representation of the preparation of *Am* leaf extract and the fabrication of *Am*-ZnO NPs. *Am*, *Annona muricata*; NaOH, Sodium hydroxide; ZnO, Zinc oxide.

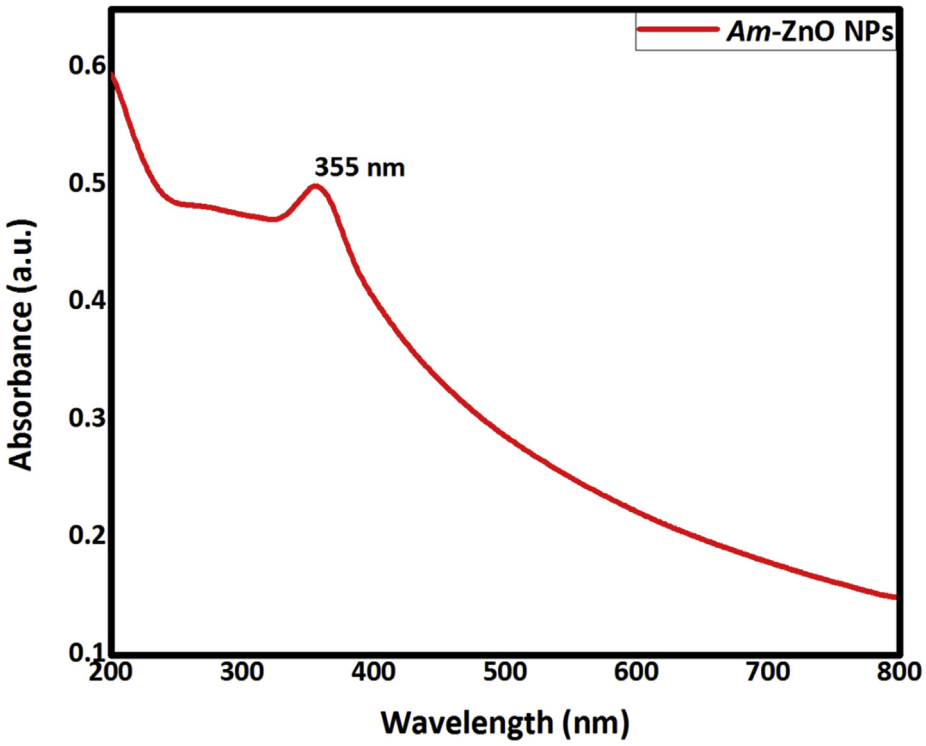

Fig. 2. UV–Visible spectral analysis of *Am*-ZnO NPs in the wavelength range of 200–800 nm.

treatment, all the steps of MMP assay were followed in a similar way as reported in our earlier study [17]. The depolarization of MMP was quantitatively measured by flow cytometry. The histogram was plotted between the doses of treatments and percentage changes in MMP.

2.3. Statistical analysis

All experimental data were analyzed using Origin 8 and GraphPad Prism 9.0 software. The obtained data represented as mean ± SD. All experiments were performed three independent

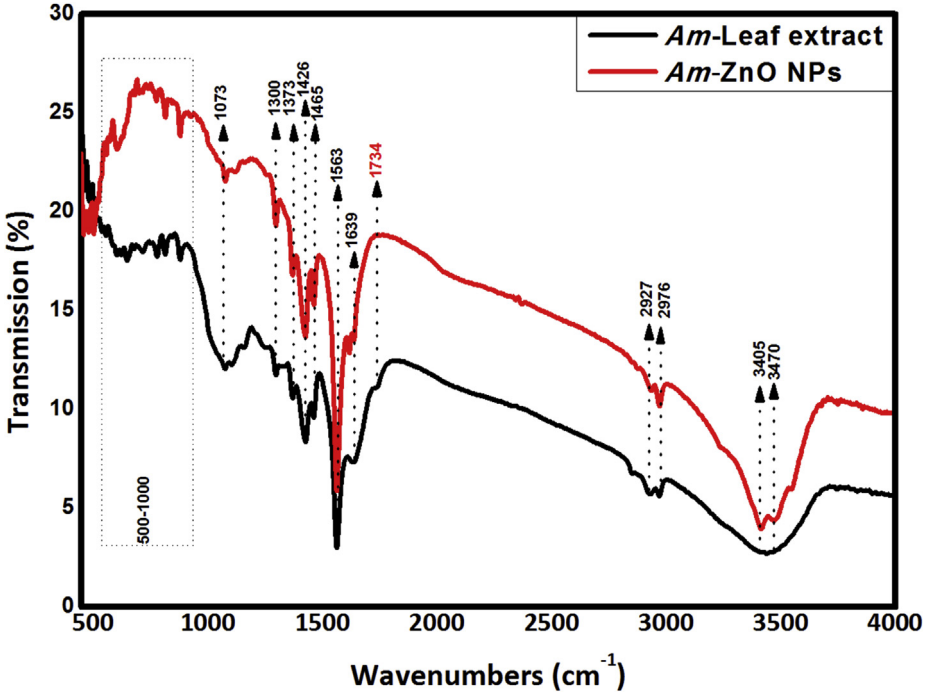

Fig. 3. FTIR spectral analysis of *Am*-leaf extract and *Am*-ZnO NPs in the wavenumber range of 4,000–500 cm^{-1}. *Am, Annona muricata; FTIR, Fourier transform infra-red.*

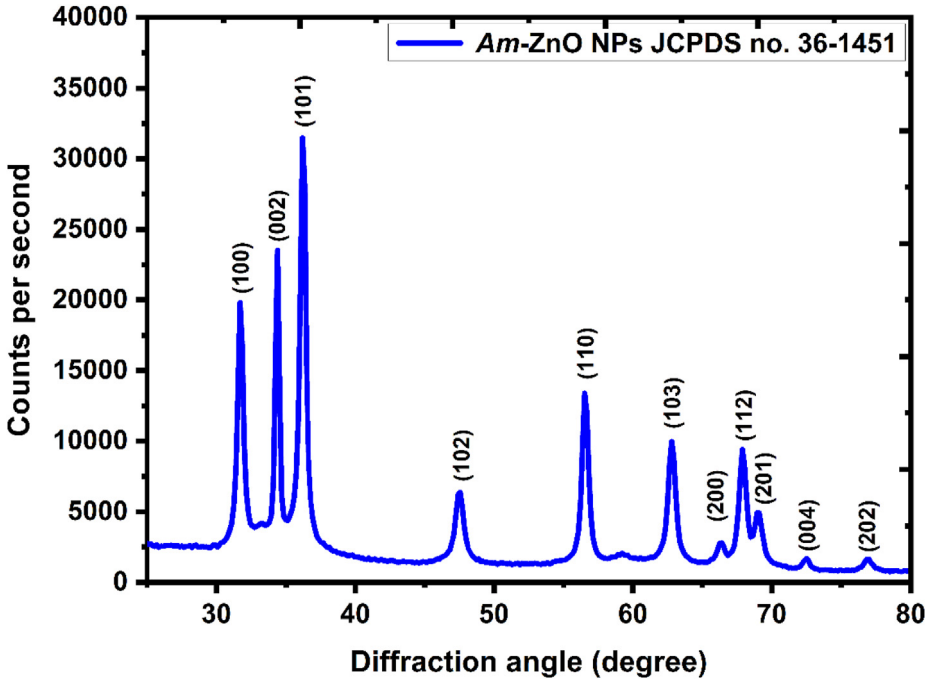

Fig. 4. XRD pattern of *Am*-ZnO NPs in the diffraction angle range of 20°–80°. XRD, X-ray diffractometer.

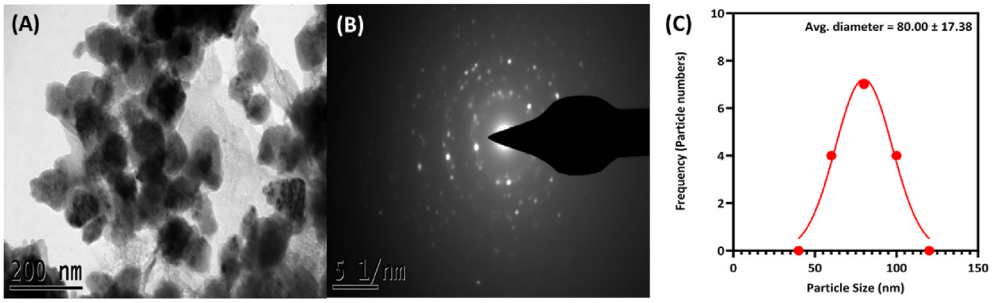

Fig. 5. (A) HR-TEM images of *Am*-ZnO NPs showing their size and shape, (B) Selected area electron diffraction analysis of *Am*-ZnO NPs, (C) The particle size distribution graph was plotted using the Gaussian Fitting curve to calculate the average particle size of *Am*-ZnO NPs. HR-TEM, high-resolution transmission electron microscopy.

times in triplicates (n = 3). *p/a<0.05 considered significant, **p/b<0.01, ***p/c<0.001, and ****p/d<0.0001.

3. Results and discussion

3.1. Fabrication and physicochemical characterizations of Am-ZnO NPs

The leaf extract of *Am* was prepared (Fig. 1), and, after adding the leaf extract solution to pale yellow solution of $Zn(CH_3COO)_2 \cdot 2H_2O$, the white precipitate was obtained. This indicated the successful synthesis of *Am*-ZnO NPs (Fig. 1) [19,39].

The UV–visible spectral analysis presented a strong peak of *Am*-ZnO NPs at 355 nm which features the intrinsic band gap of ZnO absorption (Fig. 2). In 2012, Talam et al. [20] reported a highest absorption peak of ZnO NPs at 355 nm in UV–Visible spectrum. As, in our study, the obtained absorption peak of *Am*-ZnO NPs is on similar position which supports the presence of ZnO NPs.

FTIR spectral analysis showed the possible functional groups which are responsible for the efficient stabilization of *Am*-ZnO NPs. In addition, it helped in determining the role of aqueous leaf extract of *Am* that reduced the zinc acetate into *Am*-ZnO NPs. The functional groups involved in the synthesis of *Am*-ZnO NPs showed different vibrational peaks in the range of 4,000–500 cm^{-1} (Fig. 3). In the FTIR spectrum of *Am*-ZnO NPs, two intense peaks were observed at 3,470 and 3,405 cm^{-1} corresponding to the OH group stretching. Next, two less intense peaks were seen at 2,976 cm^{-1} and 2,927 cm^{-1} attributing the CH group stretching of alkanes and OH group stretching of carboxylic group respectively. The vibrational peaks at 1,639 cm^{-1} and 1,563 cm^{-1} were assigned to the C=C stretch of alkane group and C=C stretch of aromatic rings, respectively. Next, the peaks at 1,465 cm^{-1} and 1,426 cm^{-1} represented the C=O group stretching of polyphenols. Furthermore, the emergence of peaks at 1,373 cm^{-1} and 1,300 cm^{-1} attributed to the –CO stretching and –CH bending of the alkane group. In addition, a peak at 1,073 cm^{-1} indicated the stretching of the –CN group (Fig. 3). These FTIR results were corroborated with the FTIR spectra of other plant extract–based ZnO NPs [21,22]. Our FTIR results confirmed that *Am*-ZnO NPs have functional groups of amines, alcohols, alkanes, and carboxylic acid. This suggested that phytocompounds present in *Am* leaf extract which could possibly act as the hydrolyzing agent for the ZnO NP's synthesis.

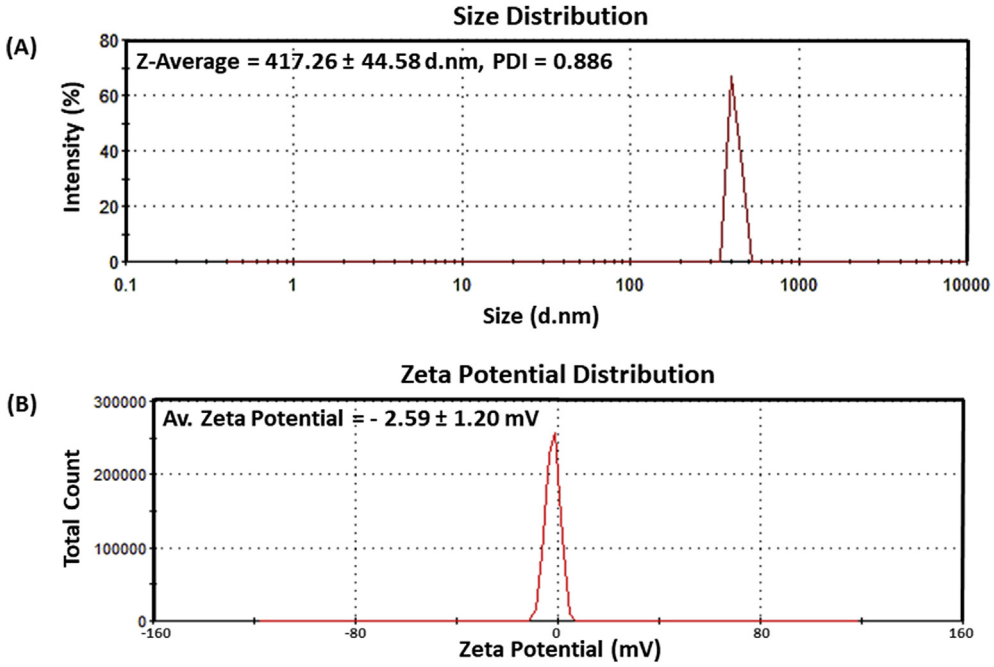

Fig. 6. (A) DLS experiment calculated the average hydrodynamic size and PDI value of *Am*-ZnO NPs; (B) Average zeta potential of *Am*-ZnO NPs calculated using Zetasizer Nano ZS instrument.

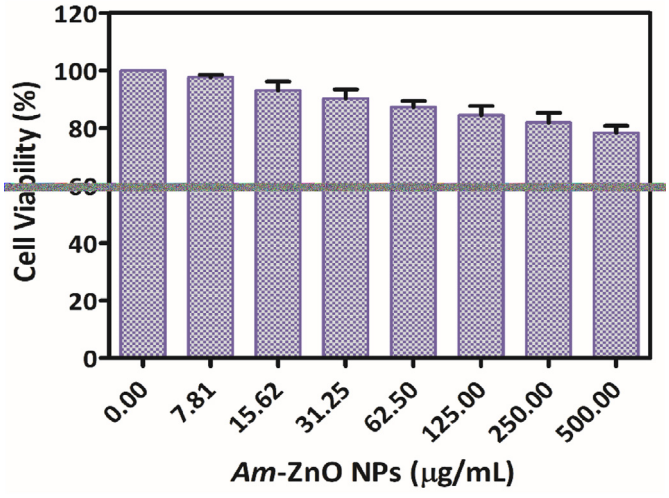

Fig. 7. Biocompatible nature of *Am*-ZnO NPs analyzed by MTT test on 3T3 cells.

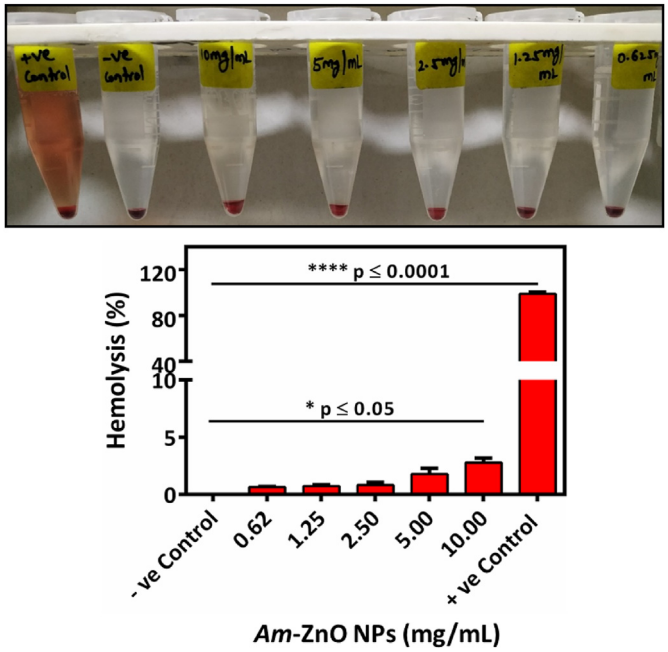

Fig. 8. Hemocompatible nature of *Am*-ZnO NPs analyzed by *in vitro* hemolysis test on 2% RBC suspension of collected blood. During the experiment, both distilled water and 1× PBS solution were used as positive and negative control, respectively. RBC, red blood cells.

Next, XRD analysis was carried out to analyze the crystalline nature of *Am*-ZnO NPs. The eleven peaks were observed at $2\theta = 31.68°$, 34.37°, 36.17°, 47.54°, 56.51°, 62.79°, 66.38°, 67.88°, 68.93°, 72.52°, and 77.00° values in the XRD pattern of *Am*-ZnO NPs. These peaks were corresponding to the (100), (002), (101), (102), (110), (103), (200), (112), (201), (004), and (202) crystal lattice planes of the hexagonal wurtzite structure of *Am*-ZnO NPs, respectively (JCPDS card no. 36-1451) (Fig. 4). In 2018, Jamdagni et al. [16] reported the highest diffraction peak of *Nat*-ZnO NPs with similar crystal plane (101) that was observed in our XRD result. In addition, the XRD pattern of *Am*-ZnO NPs did not show any diffraction peaks for zinc acetate indicating their purity without any contamination (Fig. 4). Furthermore, the average crystallite size of *Am*-ZnO NPs was calculated using the Debye–Scherrer equation [16] which was approximately 16.79 nm.

The size and shape of *Am*-ZnO NPs were analyzed by HR-TEM and FE-SEM. The *Am*-ZnO NPs were found to be nearly spherical in shape (Figs. 5A, S3). Some NPs were transparent, and some were found to be thick due to the overlapping of NPs [21]. The average particle size of these NPs was calculated to be 80.00 ± 17.38 nm (Fig. 5C). Furthermore, SAED analysis displayed the bright spots containing ring-like diffraction patterns corresponding to the

Table 1
IC_{50} values of *Am*-ZnO NPs, ZnO NPs, and DOX-HCl calculated by plotting their dose-responsive graphs. *Am*, *Annona muricata*; ZnO, zinc oxide; NPs, nanoparticles; DOX-HCl, doxorubicin hydrochloride; IC50, half maximal inhibitory concentration; A549, lung cancer cells; MOLT4, acute lymphoblastic leukemia cells.

Tested Compounds	IC_{50} values at 24 h (μg/mL)	
	A549 cells	MOLT4 cells
Am-ZnO NPs	96.67 ± 10.75	60.13 ± 7.13
DOX-HCl	0.48 ± 0.03	1.97 ± 0.45
ZnO NPs	116.91 + 2.06	150.70 ± 6.40

different crystal lattice planes of *Am*-ZnO NPs. This analysis concluded the crystalline nature of *Am*-ZnO NPs (Fig. 5B). These similar observations were reported in the previous study by Nagajyothi et al. [23] and Rajiv et al. [24].

The average hydrodynamic size ($Z_{Average}$) and PDI values of *Am*-ZnO NPs were calculated to be 417.26 ± 44.58 d nm and 0.886 ± 0.213, respectively (Fig. 6A). The average hydrodynamic size of *Am*-ZnO NPs was calculated by the DLS experiment. Those values are always higher compared to the average particle size calculated using the transmission electron microscopy (TEM) image because the size of NPs measured during TEM analysis in the dry state however, in DLS, the size of NPs measured in the aqueous state which makes a hydration layer around the surface of NPs [25]. The average hydrodynamic size of *Am*-ZnO NPs was found to be higher because of the aggregation or agglomeration of NPs [26]. Prior to their use in biomedical applications, the *Am*-ZnO NPs were probe sonicated at 30 Hz for 30 min to obtain their less aggregated state. Next, the average zeta potential of *Am*-ZnO NPs was calculated to be − 2.59 ± 1.20 mV (Fig. 6B). According to the DLVO theory, the less zeta potential value indicates a weak repulsive force between the NPs and promotes aggregation [25]. The net negative charge on the surface of *Am*-ZnO NPs is due to the strong binding affinity of phytocompounds with NPs. This conferred the stability of *Am*-ZnO NPs [27].

The stability of *Am*-ZnO NPs was studied in 10% serum containing DMEM media for 15 days. During the experiment, the average hydrodynamic size and PDI values of these NPs were calculated at each 5 days' time interval. We observed no significant differences in the $Z_{average}$ and PDI values with respect to time indicating *Am*-ZnO NPs are stable in nature (Figure S4). As it is well known that most of the serum proteins possess the net negative charge on their surface. When they come in contact with *Am*-ZnO NPs then these NPs might arise repulsions which prevents the formation protein corona around these NPs [44].

3.2. Biocompatibility and hemocompatibility

The biocompatible nature of *Am*-ZnO NPs was studied by MTT test on 3T3 cells. The cell viability of treated 3T3 cells was found to be more than 80% on different concentrations of *Am*-ZnO NPs (Fig. 7). This test concluded the improved biocompatibility of *Am*-ZnO NPs [28]. The IC_{50} value of *Am*-ZnO NPs could not be calculated as the treated 3T3 cells did not display 50% cell death in 72 h (Fig. 7). However, the cytotoxic effects of these NPs depend upon various factors such as, shape, size, and synthesis methods of NPs, and the type of cell lines used [29].

Next, RBCs were incubated with different concentrations of *Am*-ZnO NPs along with the positive and negative controls. No hemolysis or release of hemoglobin in the solution was observed except the positive control during the hemocompatibility test. The percentages of hemolysis for the negative control, positive control, 0.62, 1.25, 2.50, 5.0, and 10.0 mg/mL concentrations of *Am*-ZnO NPs were calculated to be 0.00 ± 0.00%, 98.94 ± 1.49%, 0.63 ± 0.06%, 0.72 ± 0.11%, 0.82 ± 0.23%, 1.78 ± 0.49%, and 2.78 + 0.39%, respectively (Fig. 8). These observations could be seen due to the

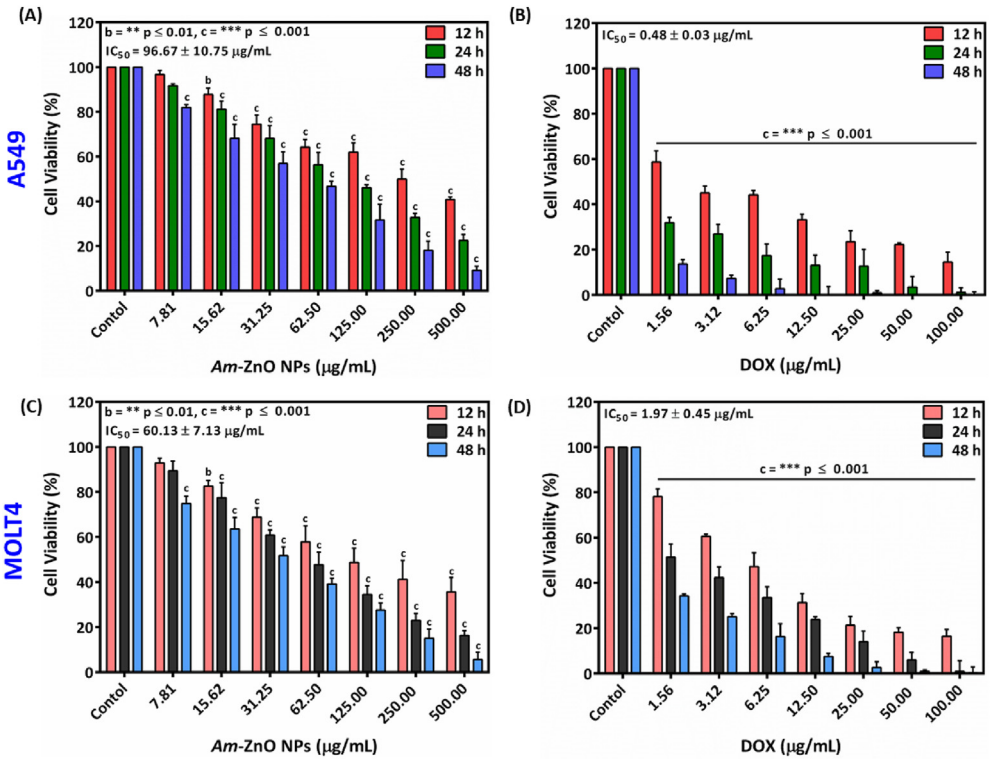

Fig. 9. Anticancer effects of *Am*-ZnO NPs and DOX-HCl analyzed against A549 and MOLT4 cells (2D tumor models) in a dose-dependent manner for 12, 24, and 48 h. The IC_{50} values of both treatments were calculated by plotting their dose-responsive graphs.

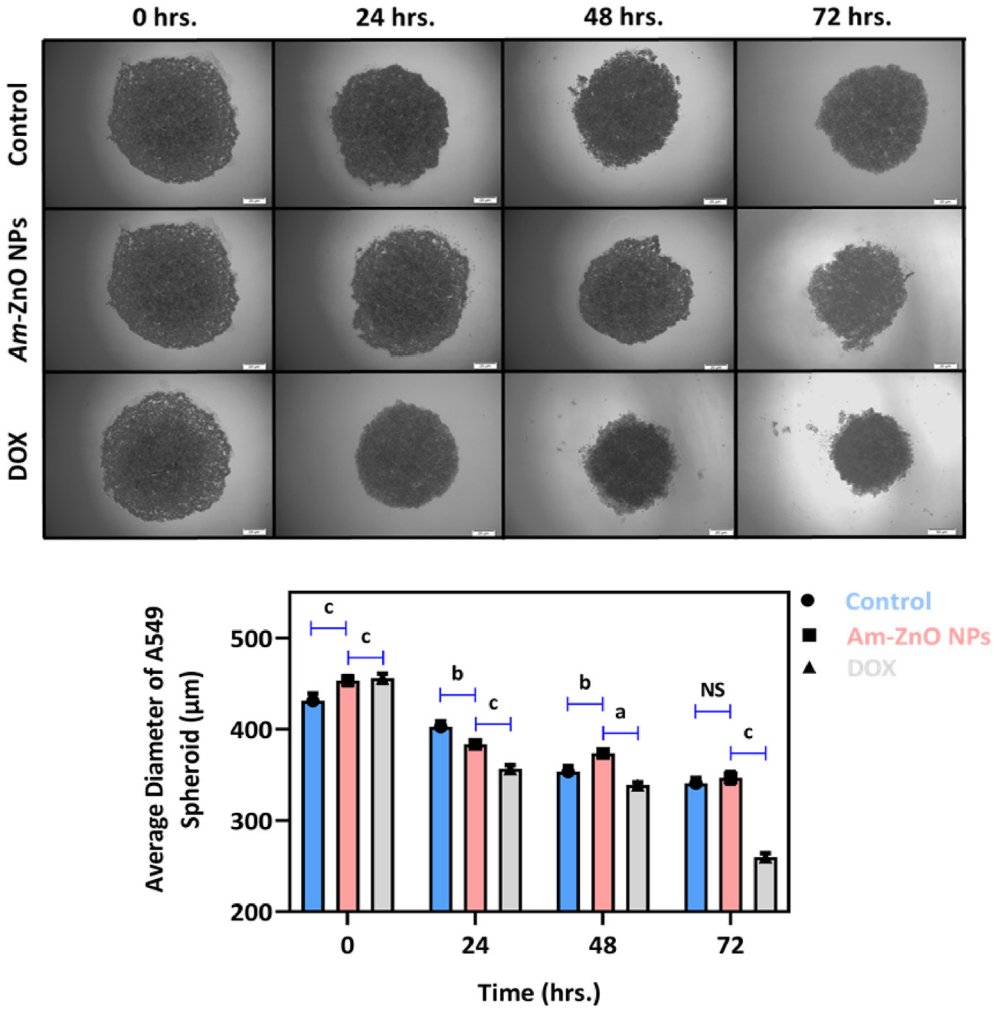

Fig. 10. Anticancer effects of *Am*-ZnO NPs and DOX-HCl analyzed on A549 tumor spheroids (3D tumor model) for 24, 48, and 72 h. The diameter of each A549 tumor spheroid was calculated using Image J software (NIH, USA) in both negative control (untreated A549 spheroids) and other treatments. The histogram was plotted between the average diameter of A549 spheroids and time (h).

presence of similar negative charges on the surface of NPs and RBCs. In result, these NPs could not interact with RBCs due to repulsive forces thus prevented RBC lysis and hemoglobin did not release in the PBS solution [29]. If the percentage of hemolysis is $\geq$ 5%, then the tested compound is hemolytic in nature; however, if the percentage of hemolysis is <5% then the tested compound is non-hemolytic. Thereby, the *Am*-ZnO NPs have good hemocompatibility even at its higher concentration, and it has been considered safe for intravenous injection with enough safety for clinical application [30]. Similarly, we also tested the hemocompatibility of ZnO NPs, and it was also found to be hemocompatible in nature (Figure S1). Based on these results, *Am*-ZnO NPs are highly biocompatible and hemocompatible in nature and can be used in various biomedical applications.

3.3. Anticancer effects on 2D and 3D tumor models

The anticancer effects of ZnO NPs and *Am*-ZnO NPs were investigated primarily on 2D tumor models such as A549 and MOLT4 cells. During the experiment, the DOX-HCl treatment to both cancer cells were kept as the positive control. The anticancer study was carried out using the MTT test in a dose-dependent manner till 48 h. In case of *Am*-ZnO NP—treated A549 and MOLT4 cells, the percentages of cell viability were calculated for negative control, 7.81, 15.62, 31.25, 62.50, 125, 250, and 500 µg/mL concentrations of NPs at 12, 24, and 48 h. The obtained results are showed in Table S1 and S2 (as given in Supplementary information). Similarly, the percentages of cell viability were also calculated only at 24 h in ZnO NP—treated A549 and MOLT4 cells on the given aforementioned concentrations. The obtained results are given in Table S5 and S6 (as given in Supplementary information). Next, we calculated the cell viability for DOX-HCl on negative control, 1.56, 3.12, 6.25, 12.50, 25, 50, and 100 µg/mL concentrations at similar time-intervals (12, 24, and 48 h) in DOX-HCl—treated A549 and MOLT4 cells. The obtained results are showed in Table S3 and S4 (as given in Supplementary information). From these results, the IC_{50} values of ZnO NPs, *Am*-ZnO NPs, and DOX-HCl were calculated at 24 h as shown in Table 1. In this test, DOX-HCl treatment was used to analyze the anticancer effects of both ZnO NPs and *Am*-ZnO NPs. The IC_{50} values of DOX-HCl were calculated to be very low as compared to the IC_{50} values of ZnO NPs and *Am*-ZnO NPs as given in Table 1.

This observation could conclude that DOX-HCl is highly toxic to both cancer cells on different concentrations (Fig. 9B, D). Furthermore, the anticancer effect of *Am*-ZnO NPs was seen higher against MOLT4 cells compared to A549 cells (Fig. 9A, C). In addition, the different concentrations of *Am*-ZnO NPs displayed the significant toxicity to both cancer cells (Fig. 9A, C). Similarly, ZnO NPs showed

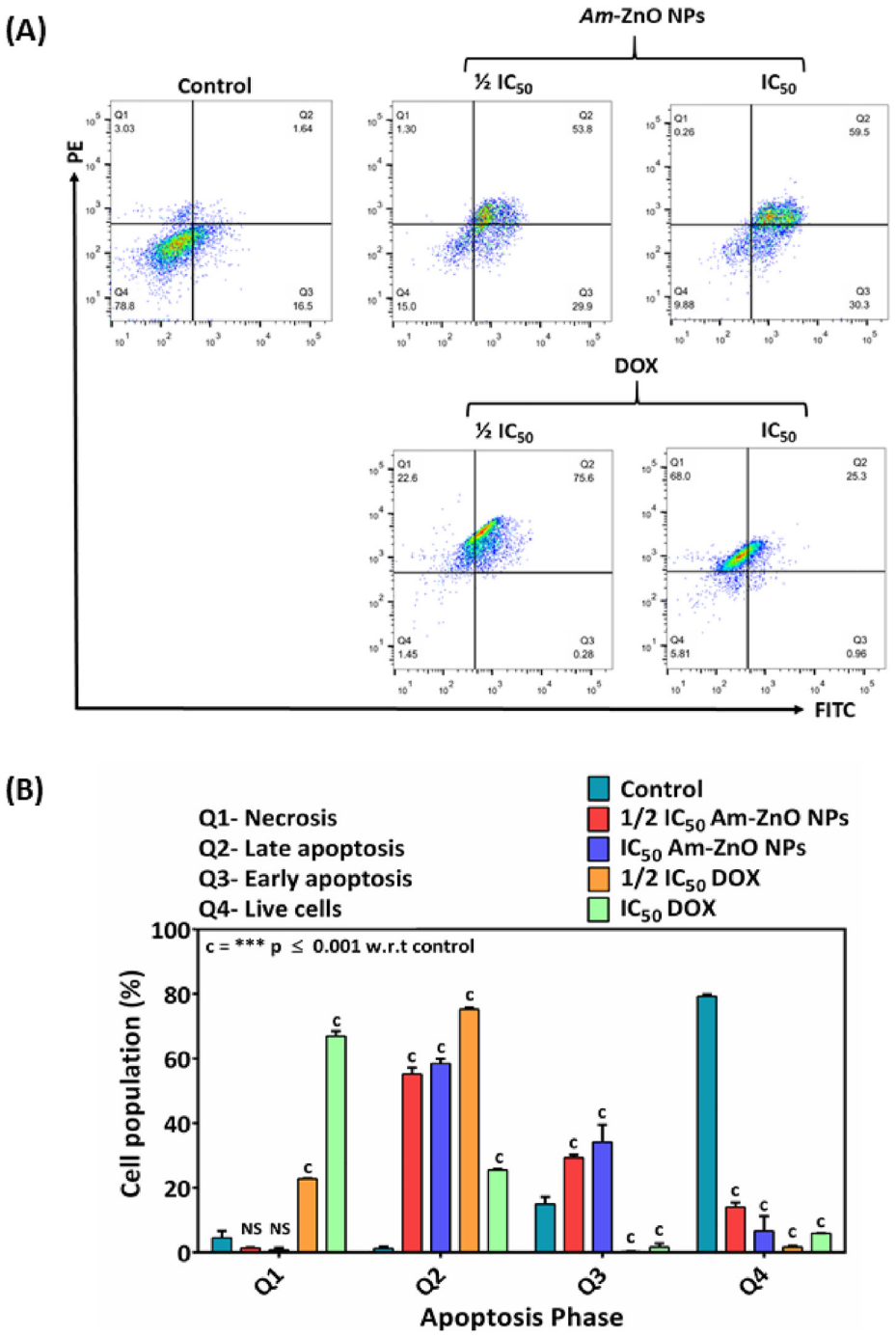

Fig. 11. (A) Apoptosis study carried out by flow cytometry using Annexin V-FITC/PI staining kit on A549 cells. These cells were treated with ½ IC_{50} and IC_{50} values of DOX-HCl and *Am*-ZnO NPs. BD FACSDIVA 8.0.1 software used to analyze the total percentages of live, early apoptotic, late apoptotic, and necrotic cells. (B) The X and Y axis in histogram indicate the different phases of apoptosis and the percentages of cancer cell population, respectively.

the anticancer effects against both cancer cells; however, these NPs displayed higher cytotoxicity against A549 cells than MOLT4 cells (Figure S2). Based on these observations, *Am*-ZnO NPs displayed higher anticancer effects than ZnO NPs because of the bioactive compounds present on the surface of *Am*-ZnO NPs. The similar results for the anticancer effects of biogenic ZnO NPs were reported previously in several other studies. In 2019, Hussain et al. [31] fabricated ZnO NPs using the aqueous leaf extract of *Pandanus odorifer* plant and evaluated its anticancer activity by MTT test at different doses in MCF-7, HepG2, and A549 cells. The results suggested that the synthesized ZnO NPs inhibited the growth of cancer cell, when applied a concentration from 50 to 100 μg/mL [31]. In 2020, Nilavukkarasi et al. [32] synthesized nanosized ZnO NPs using the leaf extract of *Capparis zeylanica* plant, and their cytotoxic results displayed the antiproliferative property of ZnO NPs against A549 cancer cells.

The 3D tumor model (spheroids) is the best *ex vivo* model for the anticancer drug screening because their structure mimics with the tumor microenvironment of a solid cancer. Such screening has reduced the *in vivo* testing of anticancer drugs [33]. Thereby, we

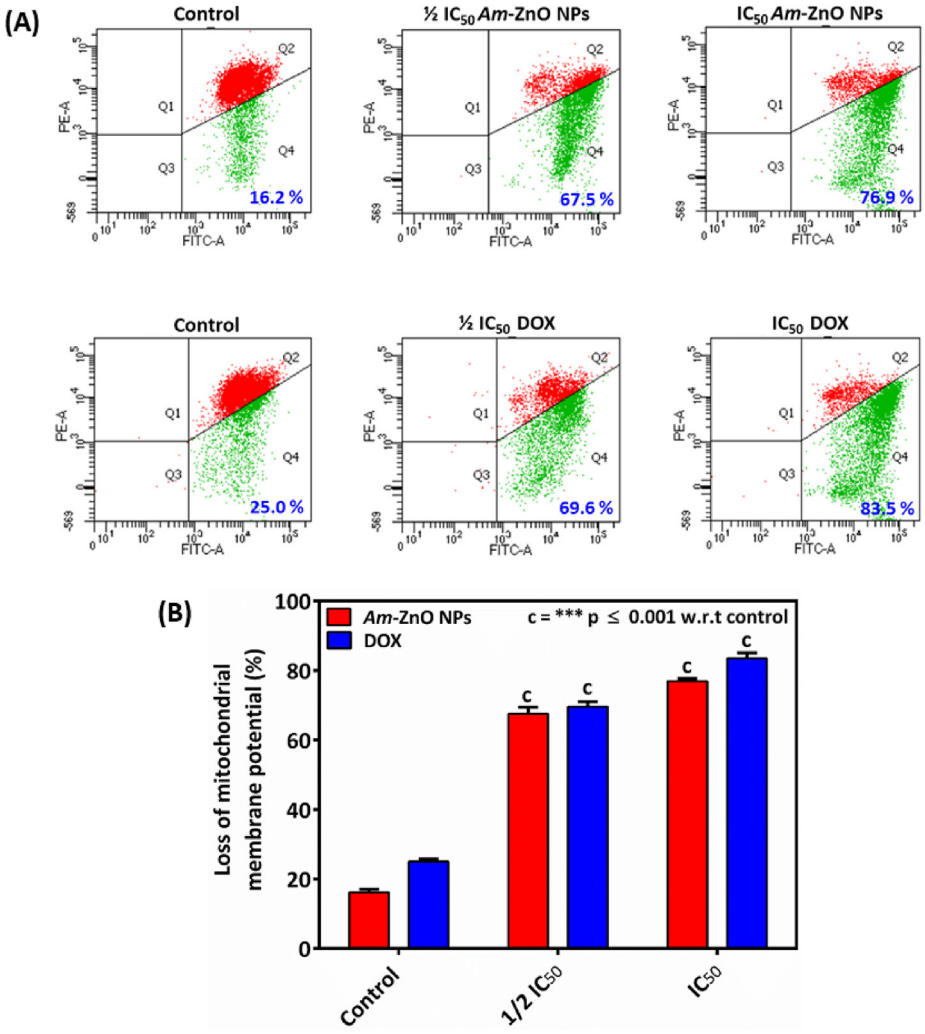

Fig. 12. (A) The change in MMP (ΔΨm) analyzed by flow cytometry using JC-1 dye in A549 cells. The cells were treated with ½ IC_{50} and IC_{50} values of DOX-HCl and *Am*-ZnO NPs. BD FACSDIVA 8.0.1 software used to analyze the MMP data. (B) The X and Y axis in the histogram indicate the different doses of DOX and *Am*-ZnO NPs treatment and the percentage loss of MMP respectively.

also investigated the anticancer effects of both *Am*-ZnO NPs and DOX-HCl on A549 tumor spheroids (3D tumor model). A significant reduction in the diameter of *Am*-ZnO NPs and DOX-HCl—treated A549 tumor spheroids was observed when compared with negative control (untreated spheroids) (Fig. 10). The average diameters of *Am*-ZnO NP—treated A549 spheroids at 0, 24, 48, and 72 h were calculated to be 453.33 ± 4.98, 383.33 ± 4.10, 373.33 ± 3.85, and 347.00 ± 6.16 μm, respectively. Similarly, the average diameters of DOX-HCl—treated A549 spheroids at 0, 24, 48, and 72 h were calculated to be 456.00 ± 4.89, 356.66 ± 3.85, 339.00 ± 2.94, and 259.66 ± 4.49 μm, respectively. However, in control, the average diameters of A549 spheroids at 0, 24, 48, and 72 h were calculated to be 431.00 ± 8.28, 402.66 ± 6.12, 353.66 ± 5.79, and 340.66 ± 6.12 μm, respectively (Fig. 10). From these observations, it was found that the *Am*-ZnO NPs have strong anticancer activity. In this study, DOX-HCl was used to analyze the anticancer effect of *Am*-ZnO NPs on A549 spheroids. In control, we also observed a reduction in the average diameter of A549 spheroids which may be due to the depletion of nutrients in the culture medium [34]. These results corroborated the cell viability data of *Am*-ZnO NPs on 2D tumor models. However, the observations of our *ex vivo* results will be validated in future on *in vivo* tumor models. Previously, in 2017, Wang et al. [35] fabricated ZnO/Dox NPs possessing excellent pH-responsive drug-release property. These NPs were effectively penetrated in 3D tumor spheroids compared with free Dox and displayed high cytotoxicity in tumor spheroids [35]. Similarly, in 2021, Dang et al. [36] synthesized ZnO spiky NPs. These NPs exhibited superior anticancer activity on 3D tumor cell spheroids.

3.4. Evaluation of cancer cell death mechanism

The mechanism of cancer cell death was investigated by the apoptosis study. The percentages of apoptotic cells were analyzed by flow cytometry in A549 cells (Fig. 11A). After the treatments of *Am*-ZnO NPs and DOX-HCl, the total percentages of apoptotic cells were analyzed at 24 h. The total percentages of live cells, apoptotic cells, and necrotic cells in case of ½ IC_{50} and IC_{50} values of *Am*-ZnO NPs were calculated to be 14.05%, 84.55%, 1.40% and 6.66%, 92.55%, 0.76%, respectively (Fig. 11B).

Similarly, the total percentages of live cells, apoptotic cells, and necrotic cells in case of ½ IC_{50} values of DOX-HCl were calculated to be 1.68%, 75.49%, and 22.75% and and for IC_{50} values were 5.88%, 27.2%, and 66.95%, respectively (Fig. 11B). Moreover, in the negative control, the total percentages of live cells, apoptotic cells, and necrotic cells were calculated to be 79.22%, 16.22%, and 4.54%,

respectively (Fig. 11B). These results were validating the MTT data on A549 cancer cells. From these observations, we concluded that cancer cells were undergoing death because of apoptosis mechanism. Like DOX-HCl, *Am*-ZnO NPs were also inducing the apoptosis in cancer cells. Previously, in 2017, Bai et al. [37] used ZnO NPs and studied the apoptosis inducing effects of these NPs in SKOV3 cells. They showed the round and non-adhered cancer cells in the culture medium which exhibited the characteristic apoptotic feature, and a depolarization in the MMP of ZnO NP−treated cancer cells was observed. Furthermore, they observed an upregulation of p53 and LC3 genes which indicated the upregulation of both apoptosis and autophagy mechanisms [37]. Similarly, in 2020, Wang et al. [38] evaluated the molecular mechanism of cancer cell death induced by ZnO NPs in Ca9-22 and OECM-1 cells. They showed that ZnO NPs activated the cancer cell death by apoptosis through caspase cascade. In addition, they observed a decrease in MMP of both Ca9-22 and OECM-1 cells [38]. In 2021, Hadisaputri et al. [43] prepared the ethanolic extract of *Am* leaves and evaluated its antiproliferation and cytotoxic activity on MCF7 cells. They observed an increased cytotoxic activity by changes in the morphology of cancer cells and found the shrinkage of nucleus and loss of cell membrane in MCF7 cells undergoing apoptosis. The mechanisms that mediate the apoptosis in MCF7 cells through a decrease in Bcl-2 mRNA expression and an increase in caspase-3 and caspase-9 mRNA expression. In general, Bcl-2 protein affects the permeability of the mitochondrial membrane, and this will result in the release of cytochrome c. Therefore, a decreased expression of Bcl-2 will result in the induction of apoptosis as the mitochondrial release of cytochrome c is no longer inhibited due to which the depolarization can be seen in the MMP. This will further activate the caspase pathways to produce caspase-3 as apoptotic executors [43].

Next, the depolarization in MMP indicates the induction of cellular apoptosis. Such changes were detected by flow cytometry at 24 h in *Am*-ZnO NP− and DOX-HCl−treated A549 cells (Fig. 12A). The percentages of change in MMP of A549 cells treated with ½ IC_{50} and IC_{50} values of *Am*-ZnO NPs were calculated to be 67.55 ± 1.91% and 76.95 ± 0.78%, respectively. Similarly, the percentages of change in MMP of A549 cells treated with ½ IC_{50} and IC_{50} values of DOX-HCl were calculated to be 69.60 ± 1.41% and 83.50 ± 1.56%, respectively (Fig. 12B). Moreover, in case of the negative control (untreated cells), the calculated percentages of change in MMP were 16.20 ± 0.85% and 25.05 ± 0.78%. These results concluded that *Am*-ZnO NPs and DOX-HCl treatments displayed a larger change in MMP of A549 cells than untreated A549 cells. In addition, *Am*-ZnO NPs strongly induced the programmed cell death or apoptosis in A549 cell populations when compared with the anticancer effects of DOX-HCl taken as positive control. Previously, the similar results were reported by other studies [37,38].

4. Conclusions

Zinc oxide NPs have been widely used in bioelectronics, biosensing, bioimaging, drug delivery, and tissue engineering applications because of their non-toxic nature. In this study, we first-time fabricated biogenic ZnO NPs using the aqueous leaf extract of *Am* plant. The *Am*-ZnO NPs were physicochemically characterized by different spectroscopy and microscopy techniques. The FTIR and UV−visible spectrum exhibited the preparation and optical nature of *Am*-ZnO NPs, respectively. High-resolution transmission electron microscopy analysis displayed the nearly spherical shape of *Am*-ZnO NPs. The zeta potential measurement presented the net negative charge on the surface of NPs. These NPs can be used broadly because of their biocompatible and hemocompatible nature. Furthermore, the fabricated *Am*-ZnO NPs showed the strong anticancer activity on both 2D and 3D tumor models. Subsequently, the *Am*-ZnO NP−treated cancer cells underwent programmed cell death with depolarization in their MMP. These results showed that biogenic ZnO NPs possess the excellent property for their broader biomedical use. In future, this nanomaterial will be tested for their subacute and system toxicity in a rodent model.

Credit author statement

Siva Chander Chabattula: Conceptualization, Writing − review & editing, **Piyush Kumar Gupta**: Conceptualization, Writing − review & editing, Supervision, Visualization, Project administration, Funding acquisition, **Surya Kant Tripathi:** Writing − review & editing, **Rekha Gahtori:** Writing − review & editing, **Priyadarshini Padhi:** Writing − review & editing, **Sujata Mahapatra:** Writing − review & editing, **R. Ranjithkumar:** Writing − review & editing, **Bijesh Kumar Biswal:** Writing − review & editing, **Sachin Kumar Singh:** Writing − review & editing, **Kamal Dua:** Review & Editing, **Janne Ruokolainen:** Review & Editing, **Yogendra Kumar Mishra:** Writing − review & editing. **Niraj Kumar Jha:** Writing − review & editing, **Dillip Kumar Bishi:** Conceptualization, Project administration, Funding acquisition, **Kavindra Kumar Kesari:** Writing − review & editing, Supervision.

Declaration of competing interest

Authors declare no known competing financial interests or personal relationships that could have appeared to influence the work reported in this paper.

Acknowledgements

Dr. Piyush Kumar Gupta is thankful to Sharda University for the infrastructure and facility. We are also thankful to Dr. Dharanivasan Gunasekaran, Agricultural Research Organization, Israel for assisting to take the TEM and SAED images of ZnO nanoparticles. Dr. Dillip Kumar Bishi is thankful to Rama Devi Women's University for the Infrastructure and facility. DKB acknowledges the funding support from Science and Engineering Research Board (SERB), Department of Science and Technology, Govt. of India for the 'Start-up Research Grant − 2019' (SRG/2019/001995).

Appendix A. Supplementary data

Supplementary data to this article can be found online at https://doi.org/10.1016/j.mtchem.2021.100618.

References

[1] I. Khan, K. Saeed, I. Khan, Nanoparticles: properties, applications and toxicities, Arab. J. Chem. 12 (2019) 908−931, https://doi.org/10.1016/j.arabjc.2017.05.011.
[2] J.J. Giner-Casares, M. Henriksen-Lacey, M. Coronado-Puchau, L.M. Liz-Marzan, Inorganic nanoparticles for biomedicine: where material scientists meet medical research, Mater. Today 19 (2016) 19−28, https://doi.org/10.1016/j.mattod.2015.07.004.
[3] M.Z. Ahmad, S. Akhter, G.K. Jain, M. Rahman, S.A. Pathan, F.J. Ahmad, R.K. Khar, Metallic nanoparticles: technology overview and drug delivery applications in oncology, Expert Opin. Drug Deliv. 7 (2010) 927−942, https://doi.org/10.1517/17425247.2010.498473.
[4] M.P. Nikolova, M.S. Chavali, Metal oxide nanoparticles as biomedical materials, Biomimetics 5 (2020) 27, https://doi.org/10.3390/biomimetics5020027.
[5] J. Singh, T. Dutta, K.H. Kim, M. Rawat, P. Samddar, P. Kumar, Green synthesis of metals and their oxide nanoparticles: applications for environmental remediation, J. Nanobiotechnol. 16 (2018) 84, https://doi.org/10.1186/s12951-018-0408-4.
[6] A.M. El shafey, Green synthesis of metal and metal oxide nanoparticles from plant leaf extracts and their applications: a review, Green Process. Synth. 9 (2020) 304−339, https://doi.org/10.1515/gps-2020-0031.

[7] J. Jeevanandam, Y.S. Chan, M.K. Danquah, Biosynthesis of metal and metal oxide nanoparticles, ChemBioEng Rev. 3 (2016) 55–67, https://doi.org/10.1002/cben.201500018.
[8] A.S. Choudhari, P.C. Mandave, M. Deshpande, P. Ranjekar, O. Prakash, Phytochemicals in cancer treatment: from preclinical studies to clinical practice, Front. Pharmacol. 10 (2020) 1614, https://doi.org/10.3389/fphar.2019.01614.
[9] G.R.K.S. Mohammad, M.H. Tabrizi, T. Ardalan, S. Yadamani, E. Safavi, Green synthesis of zinc oxide nanoparticles and evaluation of anti-angiogenesis, anti-inflammatory and cytotoxicity properties, J. Biosci. 44 (2019) 30, https://doi.org/10.1007/s12038-019-9845-y.
[10] S.Z. Moghadamtousi, M. Fadaeinasab, S. Nikzad, G. Mohan, H.M. Ali, H.A. Kadir, *Annona muricata* (Annonaceae): a review of its traditional uses, isolated acetogenins and biological activities, Int. J. Mol. Sci. 16 (2015) 15625–15658, https://doi.org/10.3390/ijms160715625.
[11] C.A. Pieme, S.G. Kumar, M.S. Dongmo, B.M. Moukette, F.F. Boyoum, J.Y. Ngogang, A.K. Saxena, Antiproliferative activity and induction of apoptosis by *Annona muricata* (Annonaceae) extract on human cancer cells, BMC Compl. Altern. Med. 14 (2014) 516, https://doi.org/10.1186/1472-6882-14-516.
[12] J.C. Chamcheu, I. Rady, R.C.N. Chamcheu, A.B. Siddique, M.B. Bloch, S.B. Mbeumi, A.S. Babatunde, M.B. Uddin, F.K. Noubissi, P.W. Jurutka, Y.Y. Liu, V.S. Spiegelman, G.K. Whitfield, K.A.E. Sayed, Graviola (*Annona muricata*) exerts anti-proliferative, anti-clonogenic and pro-apoptotic effects in human non-melanoma skin cancer UW-BCC1 and A431 cells in vitro: involvement of hedgehog signaling, Int. J. Mol. Sci. 19 (6) (2018) 1791, https://doi.org/10.3390/ijms19061791.
[13] K.M. Ezealisiji, X.S. Noundou, S.E. Ukwueze, Green synthesis and characterization of monodispersed silver nanoparticles using root bark aqueous extract of *Annona muricata* Linn and their antimicrobial activity, Appl. Nanosci. 7 (2017) 905–911, https://doi.org/10.1007/s13204-017-0632-5.
[14] M. Sabapati, N.N.C.K. Palei, A. Kumar, R.B. Molakpogu, Solid lipid nanoparticles of *Annona muricata* fruit extract: formulation, optimization and in vitro cytotoxicity studies, Drug Dev. Ind. Pharm. 45 (2019) 577–586, https://doi.org/10.1080/03639045.2019.1569027.
[15] S.U.F.S. Najmuddin, M.F. Romli, M. Hamid, N.B. Alitheen, N.M.A.N.A. Rahman, Anti-cancer effect of *Annona muricata* Linn leaves Crude Extract (AMCE) on breast cancer cell line, BMC Compl. Altern. Med. 16 (2016) 311, https://doi.org/10.1186/s12906-016-1290-y.
[16] P. Jamdagni, P. Khatri, J.S. Rana, Green synthesis of zinc oxide nanoparticles using flower extract of *Nyctanthes arbor-tristis* and their antifungal activity, J. King Saud Univ. Sci. 30 (2018) 168–175, https://doi.org/10.1016/j.jksus.2016.10.002.
[17] P.K. Gupta, S. Pappuru, S. Gupta, B. Patra, D. Chakraborty, R.S. Verma, Self-assembled dual-drug loaded core-shell nanoparticles based on metal-free fully alternating polyester for cancer theranostics, Mater. Sci. Eng. C 101 (2019) 448–463, https://doi.org/10.1016/j.msec.2019.03.041.
[18] P.K. Gupta, S.K. Tripathi, S. Pappuru, S.C. Chabattula, K. Govarthanan, S. Gupta, B.K. Biswal, D. Chakraborty, R.S. Verma, Metal-free semi-aromatic polyester as nanodrug carrier: a novel tumor targeting drug delivery vehicle for potential clinical application, Mater. Sci. Eng. C 107 (2020) 110285, https://doi.org/10.1016/j.msec.2019.110285.
[19] S. Rajeshkumar, S.V. Kumar, A. Ramaiah, H. Agarwal, T. Lakshmi, S.M. Roopan, Biosynthesis of zinc oxide nanoparticles using *Mangifera indica* leaves and evaluation of their antioxidant and cytotoxic properties in lung cancer (A549) cells, Enzym. Microb. Technol. 117 (2018) 91–95, https://doi.org/10.1016/j.enzmictec.2018.06.009.
[20] S. Talam, S.R. Karumuri, N. Gunnam, Synthesis, characterization, and spectroscopic properties of ZnO nanoparticles, Int. Sch. Res. Not. 2012 (2012) 372505, https://doi.org/10.5402/2012/372505.
[21] S. Sathappan, N. Kirubakaran, D. Gunasekaran, P.K. Gupta, R.S. Verma, J. Sundaram, Green synthesis of zinc oxide nanoparticles (ZnO NPs) using cissus quadrangularis: characterization, antimicrobial, and anticancer studies, Proc. Natl. Acad. Sci. India Sect. B Biol. Sci. (2021), https://doi.org/10.1007/s40011-020-01215-w.
[22] B. Malaikozhundan, B. Vaseeharan, S. Vijayakumar, K. Pandiselvi, M.A.R. Kalanjiam, K. Murugan, G. Benelli, Biological therapeutics of Pongamia pinnata coated zinc oxide nanoparticles against clinically important pathogenic bacteria, fungi and MCF-7 breast cancer cells, Microb. Pathog. 104 (2017) 268–277, https://doi.org/10.1016/j.micpath.2017.01.029.
[23] P.C. Nagajyothi, T.V.M. Sreekanth, C.O. Tettey, Y.I. Jun, S.H. Mook, Characterization, antibacterial, antioxidant and cytotoxic activities of ZnO nanoparticles using Coptidis rhizome, Bioorg. Med. Chem. Lett 24 (2014) 4298–4303, https://doi.org/10.1016/j.bmcl.2014.07.023.
[24] P. Rajiv, S. Rajeshwari, R. Venckatesh, Bio-fabrication of zinc oxide nanoparticles using leaf extract of *Parthenium hysterophorus* L. and its size dependent antifungal activity against plant fungal pathogens, Spectrochim. Acta A Mol. Biomol. Spectrosc. 112 (2013) 384–387, https://doi.org/10.1016/j.saa.2013.04.072.
[25] S. Jafarirad, M. Mehrabi, B. Divband, M. Kosari-Nasab, Biofabrication of zinc oxide nanoparticles using fruit extract of *Rosa canina* and their toxic potential against bacteria: a mechanistic approach, Mater. Sci. Eng. C 59 (2016) 296–302, https://doi.org/10.1016/j.msec.2015.09.089.
[26] S. Rajashekara, A. Shrivastava, S. Sumhitha, S. Kumari, Biomedical applications of biogenic zinc oxide nanoparticles manufactured from leaf extracts of *Calotropis gigantea* (L.) dryand, BioNanoScience 10 (2020) 654–671, https://doi.org/10.1007/s12668-020-00746-w.
[27] S. Faisal, H. Jan, S.A. Shah, S. Shah, A. Khan, M.T. Akbar, M. Rizwan, F. Jan, Wajidullah, N. Akhtar, A. Khattak, S. Syed, Green synthesis of zinc oxide (ZnO) nanoparticles using aqueous fruit extracts of *Myristica fragrans*: their characterizations and biological and environmental applications, ACS Omega 6 (2021) 9709–9722, https://doi.org/10.1021/acsomega.1c00310.
[28] H. Jan, M. Shah, H. Usman, M.A. Khan, M. Zia, C. Hano, B.H. Abbasi, Biogenic synthesis and characterization of antimicrobial and antiparasitic zinc oxide (ZnO) nanoparticles using aqueous extracts of the Himalayan columbine (Aquilegia pubiflora), Front. Mater. 7 (2020) 249, https://doi.org/10.3389/fmats.2020.00249.
[29] H.M. Yusof, N.A. Rahman, R. Mohamad, U.H. Zaidan, A.A. Samsudin, Biosynthesis of zinc oxide nanoparticles by cell biomass and supernatant of *Lactobacillus plantarum* TA4 and its antibacterial and biocompatibility properties, Nat. Sci. Rep. 10 (2020), 19996, https://doi.org/10.1038/s41598-020-76402-w.
[30] J. Zhang, J. Han, X. Zhang, J. Jiang, M. Xu, D. Zhang, J. Han, Polymeric nanoparticles based on chitooligosaccharide as drug carriers for codelivery of all-trans-retinoic acid and paclitaxel, Carbohydr. Polym. 129 (2015) 25–34, https://doi.org/10.1016/j.carbpol.2015.04.036.
[31] A. Hussain, M. Oves, M.F. Alajmi, I. Hussain, S. Amir, J. Ahmed, M.T. Rehman, H.R. El-seedi, I. Ali, Biogenesis of ZnO nanoparticles using *Pandanus odorifer* leaf extract: anticancer and antimicrobial activities, RSC Adv. 9 (2019) 15357–15369, https://doi.org/10.1039/C9RA01659G.
[32] M. Nilavukkarasi, S. Vijayakumar, S. Prathipkumar, Capparis zeylanica mediated biosynthesized ZnO nanoparticles as antimicrobial, photocatalytic and anti-cancer applications, Mater. Sci. Energy Technol. 3 (2020) 335–343, https://doi.org/10.1016/j.mset.2019.12.004.
[33] A.S. Nunes, A.S. Barros, E.C. Costa, A.F. Moreira, I.J. Correia, 3D tumor spheroids as in vitro models to mimic in vivo human solid tumors resistance to therapeutic drugs, Biotechnol. Bioeng. 116 (2019) 206–226, https://doi.org/10.1002/bit.26845.
[34] S. Nath, G.R. Devi, Three-dimensional culture systems in cancer research: focus on tumor spheroid model, Pharmacol. Ther. 163 (2016) 94–108, https://doi.org/10.1016/j.pharmthera.2016.03.013.
[35] J. Wang, S. Lee, D. Kim, L. Zhu, Exploration of zinc oxide nanoparticles as a multitarget and multifunctional anticancer nanomedicine, ACS Appl. Mater. Interfaces 9 (2017) 39971–39984, https://doi.org/10.1021/acsami.7b11219.
[36] Z. Dang, J. Sun, J. Fan, J. Li, X. Li, T. Chen, Zin oxide spiky nanoparticles: a promising nanomaterial for killing tumor cells, Mater. Sci. Eng. C 124 (2021) 112071, https://doi.org/10.1016/j.msec.2021.112071.
[37] D. Bai, X. Zhang, G. Zhang, Y. Huang, S. Gurunathan, Zinc oxide nanoparticles induce apoptosis and autophagy in human ovarian cancer cells, Int. J. Nanomed. 2017 (2017) 6521–6535, https://doi.org/10.2147/IJN.S140071.
[38] S.W. Wang, C.H. Lee, M.S. Lin, C.W. Chi, Y.J. Chen, G.S. Wang, K.W. Liao, L.P. Chiu, S.H. Wu, D.M. Huang, L. Chen, Y.S. Shen, ZnO nanoparticles induced caspase-dependent apoptosis in gingival squamous cell carcinoma through mitochondrial dysfunction and p70S6K signaling pathway, Int. J. Mol. Sci. 21 (2020) 1612, https://doi.org/10.3390/ijms21051612.
[39] A. Jayachandran, T.R. Aswathy, A.S. Nair, Green synthesis and characterization of zinc oxide nanoparticles using Cayratia pedata leaf extract, Biochem. Biophys. Rep. 26 (2021) 100995, https://doi.org/10.1016/j.bbrep.2021.100995.
[40] P. Ramesh, K. Saravanan, P. Manogar, J. Johnson, E. Vinoth, M. Mayakannan, Green synthesis and characterization of biocompatible zinc oxide nanoparticles and evaluation of its antibacterial potential, Sens. Biosens. Res. 31 (2021) 100399, https://doi.org/10.1016/j.sbsr.2021.100399.
[41] R. Vinayagam, S. Pai, G. Murugesan, T. Varadavenkatesan, R. Selvaraj, Synthesis of photocatalytic zinc oxide nanoflowers using *Peltophorum pterocarpum* pod extract and their characterization, Appl. Nanosci. (2021), https://doi.org/10.1007/s13204-021-01919-z.
[42] R. Pachaiappan, S. Rajendran, G. Ramalingam, D.V.N. Vo, M. Priya, M. Soto-Moscoso, Green synthesis of zinc oxide nanoparticles by *Justicia adhatoda* leaves and their antimicrobial activity, Chem. Eng. Technol. 44 (2021) 551–558, https://doi.org/10.1002/ceat.202000470.
[43] Y.E. Hadisaputri, U. Habibah, F.F. Abdullah, E. Halimah, M. Mutakin, S. Megantara, et al., Antiproliferative activity and apoptotic mechanism of Soursop (*Annona muricata* L.) leaves extract and fractions on MCF7 breast cancer cells, Breast Cancer Targets and Therapy. 2021 (2021) 447–457, https://doi.org/10.2147/BCTT.S317682.
[44] S.R. Saptarshi, A. Duschl, A.L. Lopata, Interaction of nanoparticles with proteins: relation to bio-reactivity of the nanoparticle, J. Nanobiotechnol. 11 (2013) 26, https://doi.org/10.1186/1477-3155-11-26.
[45] B. Ortiz-Casas, A. Galdamez-Martinez, J. Gutierrez-Flores, A.B. lbanez, P.K. Panda, G. Santana, H.A.D.L. Vega, M. Suar, C.G. Rodelo, A. Kaushik, Y.K. Mishra, A. Dutt, Bio-acceptable 0D and 1D ZnO nanostructures for cancer diagnostics and treatment, Mater. Today. (2021), https://doi.org/10.1016/j.mattod.2021.07.025.